Journal of Sound and Vibration 329 (2010) 607–626

Contents lists available at ScienceDirect

Journal of Sound and Vibration

journal homepage: www.elsevier.com/locate/jsvi

# Influence of mean flow profile and geometrical ratios on scattering of sound at a sudden area expansion in a duct

G. Kooijman [a,*], A. Hirschberg [a], Y. Aurégan [b]

[a] Eindhoven University of Technology, Department of Applied Physics, Fluid Dynamics Laboratory, P.O. Box 513, 5600 MB, Eindhoven, The Netherlands
[b] Laboratoire d'Acoustique de l'Université du Maine, Avenue Olivier Messiaen 72085, Le Mans, Cedex 9, France

ARTICLE INFO

*Article history:*
Received 21 August 2007
Received in revised form
2 September 2009
Accepted 16 September 2009
Handling Editor: C.L. Morfey
Available online 13 October 2009

ABSTRACT

The scattering of sound at a sudden area expansion in a duct with subsonic mean flow has been modelled with a multimodal method. Technological applications are for instance internal combustion engine exhaust silencers and silencers in industrial duct systems. Both 2D rectangular and 2D cylindrical geometries are considered.

The influence of the mean flow profile, and the—in this method—associated application of an acoustic Kutta condition at the edge of the area discontinuity, is investigated. The scattering coefficients for the plane waves are found to change smoothly as the flow profile is changed gradually from one, where the acoustic Kutta condition is applied to one where it is not applied. Furthermore, for high Strouhal numbers no difference is observed in the results for the scattering coefficients obtained for different flow profiles. Also, at low Strouhal numbers the magnitudes of the scattering coefficients are the same for different profiles.

The influence of the ratio of the heights (in 2D rectangular geometry), respectively, radii (in 2D cylindrical geometry), of the ducts upstream and downstream of the area expansion on the scattering coefficients is examined. Around a certain Strouhal number, a specific feature in the scattering coefficients is observed when the ratio of the duct heights or radii is less than 0.5. This is found to be connected to a strong interaction between the first evanescent acoustic mode and the hydrodynamic instability mode. For non-uniform flow even an apparent jump between the first evanescent acoustic mode and the hydrodynamic unstable mode and a corresponding jump in scattering coefficients is observed, when employing causality analysis according to the Briggs–Bers or Crighton–Leppington procedure. This implies that in fact an absolute instability occurs.



## 1. Introduction

The scattering of sound at an area expansion in a duct carrying mean flow is of interest in technical applications such as internal combustion engine exhaust silencers and silencers in industrial duct systems. The interaction between sound and flow, which occurs in the shear layer formed downstream of the expansion, can namely result in sound absorption.

In an earlier paper by the authors [1] a multimodal method [2–6] to calculate the scattering of sound at an area expansion in a 2D rectangular or 2D cylindrical duct with either uniform or non-uniform flow was presented. For uniform flow model results were compared with those obtained by the simplified multimodal method of Aurégan [7,8] as well as

* Corresponding address. Currently at: Philips Research Laboratories, High Tech Campus 36, 5656 AE Eindhoven, The Netherlands.
*E-mail address:* gerben.kooijman@philips.com (G. Kooijman).

0022-460X/$ - see front matter © 2009 Elsevier Ltd. All rights reserved.
doi:10.1016/j.jsv.2009.09.021

those obtained by the model of Boij and Nilsson [9,10]. Generally, good agreement was found between the different models, especially for the downstream reflection coefficient. The scaling rule for the Helmholtz number, proposed by Boij and Nilsson [9], in order to compare scattering results for an area expansion in 2D rectangular and 2D cylindrical geometry at the same area expansion ratio, was found to be invalid at a critical Strouhal number. Here, a specific behaviour was found, which was reported to depend on the ratio of the duct heights, or ratio of duct radii, upstream and downstream of the expansion. In the present paper this phenomenon, which is closely connected to the behaviour of (the wavenumbers of) the modes, will be presented and discussed in more detail.

In Ref. [1] scattering results obtained by the multimodal method were also compared to experimental data presented by Ronneberger [11]. Fairly good agreement was found, and in some cases a better prediction of the experimental results by the model was observed when considering a non-uniform flow profile, rather than a uniform flow profile. In the present paper the influence of the flow profile, and more in particular the effect of the (in the multimodal method) related application of an acoustic Kutta condition is discussed. The Kutta condition allows to take into account the effect of viscosity in the otherwise frictionless model by assuming tangential flow separation. This appears to be equivalent to a removal of the singular edge behaviour which would prevail in a potential edge flow [12,13].

Besides the configurations with uniform flow and non-uniform flow, extensively dealt with in Ref. [1], an 'intermediate' third flow configuration, that of a non-uniform flow with a discontinuity in velocity at the flow to no flow interface, will be introduced in this paper. The eigenvalue problem for the modes and accompanying wavenumbers as well as the mode matching for this additional configuration will first be discussed. Next, the effect of flow configuration on the results for the scattering of plane waves at an area expansion is presented. Subsequently, the influence of the ratio of duct heights, or duct radii, upstream and downstream of the expansion, and the associated behaviour of the modes will be discussed in detail.

## 2. Multimodal method

Consider a sudden area expansion in a 2D rectangular duct, Fig. 1. The configuration is split into a duct at $x<0$ with height $h_1$ and a duct at $x>0$ with height $h_2$. The two are indicated in the figure with boxed numbers 1 and 2, respectively. In duct 1 parallel non-uniform mean flow with velocity $U(y)$ is present. The mean flow is assumed to continue as a free jet with unaltered profile in duct 2. This jet is in equilibrium surrounded by stagnant fluid. The flow has non-zero velocity at the upper wall of duct 1, resulting in a slip velocity between the flow/no flow interface in duct 2. Regarding the multimodal method this case is in fact a combination between the configuration with uniform flow and that with non-uniform flow (without slip velocity), extensively discussed in our earlier paper [1]. As shown there, starting from the linearized Euler equations for conservation of momentum and mass gives, after discretization in the $y$-direction and using finite difference for differential operators, an eigenvalue problem for the modes in duct 1:

$$k_* \begin{pmatrix} \mathbf{I}-M_0^2\mathbf{f^2} & 2\mathrm{i}M_0\mathbf{f_a} & \mathbf{0} \\ \mathbf{0} & \mathrm{i}M_0\mathbf{f} & \mathbf{0} \\ \mathbf{0} & \mathbf{0} & \mathbf{I} \end{pmatrix} \begin{pmatrix} \mathbf{Q} \\ \mathbf{V} \\ \mathbf{P} \end{pmatrix} = \begin{pmatrix} -2\omega_* M_0\mathbf{f} & \mathbf{0} & \omega_*^2\mathbf{I}+\mathbf{D_2} \\ \mathbf{0} & \mathrm{i}\omega*\mathbf{I} & \mathbf{D_1} \\ \mathbf{I} & \mathbf{0} & \mathbf{0} \end{pmatrix} \begin{pmatrix} \mathbf{Q} \\ \mathbf{V} \\ \mathbf{P} \end{pmatrix}. \tag{1}$$

Here, the following non-dimensionalization is employed:

$$p_* = \frac{1}{\rho_0 c_0^2} p', \qquad (x_*, y_*, h_{1*}, h_{2*}) = \left(\frac{x}{h_1}, \frac{y}{h_1}, 1, \frac{h_2}{h_1}\right),$$
$$(u_*, v_*) = \frac{1}{c_0}(u', v'), \qquad \omega_* = \frac{\omega h_1}{c_0},$$
$$M(y) = M_0 f(y) = \frac{1}{c_0} U(y), \qquad t_* = \frac{c_0 t}{h_1},$$

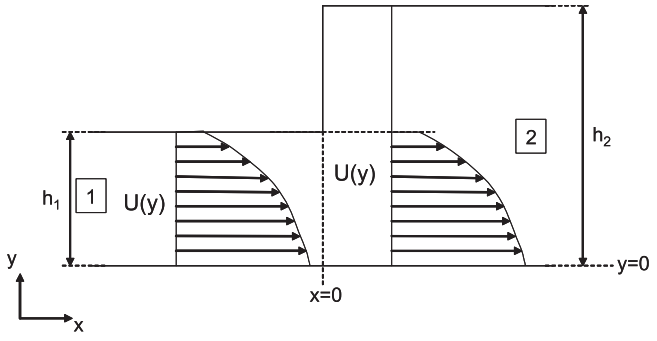


**Fig. 1.** Area expansion in a 2D rectangular duct. The configuration is split into duct 1 with height $h_1$ and duct 2 with height $h_2$. Non-uniform mean flow with a slip velocity at the upper wall is present in duct 1, the profile is unaltered in duct 2, giving a velocity jump in the shear layer.

with $p'$,$u'$, and $v'$, the linear pressure disturbance and velocity disturbance in $x$ and $y$ direction, respectively. $M_0$ is the average Mach number, $f(y)$ is a flow profile function, and $c_0$ is the speed of sound. $\omega$ is the angular frequency of sound. Harmonic waves are assumed, in complex from:

$$p_* = P(y_*)\exp(-\mathrm{i}k_*x_*)\exp(\mathrm{i}\omega_* t_*),$$

$$v_* = V(y_*)\exp(-\mathrm{i}k_*x_*)\exp(\mathrm{i}\omega_* t_*),$$

$$q_* = Q(y_*)\exp(-\mathrm{i}k_*x_*)\exp(\mathrm{i}\omega_* t_*), \tag{3}$$

with $k_*$ the dimensionless wavenumber $k_* = kh_1$, $\mathrm{i}^2 = -1$, and

$$q_* = \mathrm{i}\frac{\partial p_*}{\partial x_*}. \tag{4}$$

such that also $\mathbf{Q} = k_*\mathbf{P}$. In Eq. (1) $\mathbf{Q}$, $\mathbf{V}$ and $\mathbf{P}$ are column vectors giving the values of $Q(y_*)$, $V(y_*)$, and $P(y_*)$ at the $N_1$ discrete points in duct 1. $\mathbf{I}$ is the $(N_1 \times N_1)$ identity matrix, $\mathbf{f}$, $\mathbf{f}^2$ and $\mathbf{f}_a$ are $(N_1 \times N_1)$ matrices with on their diagonal the values of $f(y_*)$, $f^2(y_*)$ and $\mathrm{d}f(y_*)/\mathrm{d}y_*$, respectively, at the discrete points in duct 1. $\mathbf{D_1}$ and $\mathbf{D_2}$ are $(N_1 \times N_1)$ matrices giving the finite difference first, respectively, second-order differential operator with respect to $y_*$. These matrices also account for the boundary condition $\partial p_*/\partial y_* = 0$ at the duct walls. Solving the eigenvalue problem (1) gives all eigenvectors, i.e. modes, $\mathbf{Q}_e$ and $\mathbf{P}_e$ and $\mathbf{V}_e$, as well as the corresponding eigenvalues, i.e. dimensionless wavenumbers, $k_{e*}$, in duct 1. Here, in total $3N_1$ modes are found, which can be divided into $N_1$ acoustic modes propagating (or decaying) in the $+x-$direction, $N_1$ acoustic modes propagating (or decaying) in the $-x-$direction, and $N_1$ hydrodynamic modes propagating in the direction of the mean flow ($+x-$direction). The total solution for $q_*$, and the non-dimensional pressure and velocity disturbance $p_*$, respectively, $v_*$ at the discrete points is a linear combination of these modes:

$$\mathbf{q}_*(x_*,t_*) = \sum_{n=1}^{3N_1} C_n\mathbf{Q}_{e,n}\exp(-\mathrm{i}k_{e,n*}x_*)\exp(\mathrm{i}\omega_* t_*),$$

$$\mathbf{v}_*(x_*,t_*) = \sum_{n=1}^{3N_1} C_n\mathbf{V}_{e,n}\exp(-\mathrm{i}k_{e,n*}x_*)\exp(\mathrm{i}\omega_* t_*),$$

$$\mathbf{p}_*(x_*,t_*) = \sum_{n=1}^{3N_1} C_n\mathbf{P}_{e,n}\exp(-\mathrm{i}k_{e,n*}x_*)\exp(\mathrm{i}\omega_* t_*), \tag{5}$$

with $n$ an index for the modes and $C_n$ the coefficient of mode $n$.

In duct 2 a combination between the eigenvalue problem for non-uniform flow and uniform flow holds. Basically, one can start from the eigenvalue problem as in Eq. (1) where a number of rows and columns in the matrices, corresponding with equations for/with $\mathbf{V}$ at the points without mean flow have to be omitted. Subsequently, as with uniform flow, an intermediate point at the interface between mean flow and no mean flow is introduced, where the acoustic velocity in $y$ direction, with amplitudes $V_{\mathrm{flow}}$, respectively, $V_{\mathrm{noflow}}$, seen from both sides is considered, see Ref. [1]. At this intermediate point continuity of the acoustic pressure and fluid displacement is demanded. This leads to the following eigenvalue problem:

$$k_*\begin{pmatrix} \mathbf{I}-M_0^2\mathbf{f}^2 & 2\mathrm{i}M_0\mathbf{f_a} & \mathbf{0} & \mathbf{0} & \mathbf{0} \\ \mathbf{0} & \mathrm{i}M_0\mathbf{f} & \mathbf{0} & \mathbf{0} & \mathbf{0} \\ \mathbf{0} & \mathbf{0} & \mathbf{I} & \mathbf{0} & \mathbf{0} \\ \mathbf{0} & \mathbf{0} & \mathbf{0} & 3\mathrm{i}\Delta h_* M_{\mathrm{int}} & 0 \\ \mathbf{0} & \mathbf{0} & \mathbf{0} & 0 & M_{\mathrm{int}} \end{pmatrix}\begin{pmatrix} \mathbf{Q} \\ \mathbf{V} \\ \mathbf{P} \\ V_{\mathrm{flow}} \\ V_{\mathrm{noflow}} \end{pmatrix}$$

$$= \begin{pmatrix} -2\omega_* M_0\mathbf{f} & \mathbf{0} & \omega_*^2\mathbf{I}+\mathbf{D}_2 & \mathbf{0} & \mathbf{0} \\ \mathbf{0} & \mathrm{i}\omega\mathbf{I} & \mathbf{D}_1 & \mathbf{0} & \mathbf{0} \\ \mathbf{I} & \mathbf{0} & \mathbf{0} & \mathbf{0} & \mathbf{0} \\ \mathbf{0} & \mathbf{0} & \mathbf{0} & 3\mathrm{i}\Delta h_*\omega_* & 3\mathrm{i}\Delta h_*\omega_* \\ \mathbf{0} & \mathbf{0} & \mathbf{0} & -\omega_* & \omega_* \end{pmatrix}\begin{pmatrix} \mathbf{Q} \\ \mathbf{V} \\ \mathbf{P} \\ V_{\mathrm{flow}} \\ V_{\mathrm{noflow}} \end{pmatrix}, \tag{6}$$

where $M_{\mathrm{int}}$ is the (jump in) Mach number at the interface between mean flow and no mean flow. The second-order derivative of the acoustic pressure amplitude, accurate to order $(\Delta h_*)^2$, at points $N_1$ and $N_1+1$ has changed here into

$$\left.\frac{\mathrm{d}^2P}{\mathrm{d}y_*^2}\right|_{N_1} = \frac{\mathbf{P}(N_1-1)-\mathbf{P}(N_1)}{(\Delta h_*)^2} - \frac{\mathrm{i}(\omega_* - M_{\mathrm{int}}k_*)V_{\mathrm{flow}}}{\Delta h_*},$$

$$\left.\frac{\mathrm{d}^2P}{\mathrm{d}y_*^2}\right|_{N_1+1} = \frac{-\mathbf{P}(N_1+1)+\mathbf{P}(N_1+2)}{(\Delta h_*)^2} + \frac{\mathrm{i}\omega_* V_{\mathrm{noflow}}}{\Delta h_*}. \tag{7}$$

Unlike with the configuration of uniform flow, the first derivative also occurs in the eigenvalue problem for the first $N_1$ points. The first-order derivative of the acoustic pressure amplitude, accurate to order $(\Delta h_*)^2$, at point $N_1$ becomes

$$\left.\frac{\mathrm{d}P}{\mathrm{d}y_*}\right|_{N_1} = \frac{\mathbf{P}(N_1) - \mathbf{P}(N_1-1)}{2\Delta h_*} - \frac{\mathrm{i}(\omega_* - M_{\mathrm{int}}k_*)V_{\mathrm{flow}}}{2}. \tag{8}$$

These changes are taken into account in the differential matrices $\mathbf{D_1}$ and $\mathbf{D_2}$ in Eq. (6). In total $N_2$ acoustic modes propagating/decaying in the $+x-$direction and $N_2$ acoustic modes propagating/decaying in the $-x-$direction are found. Also, $N_1$ stable hydrodynamic and two unstable hydrodynamic modes are found. At the interface between duct 1 and duct 2 continuity of the parameters $q_*$, $v_*$, and $p_*$ holds. Furthermore, as in the uniform flow case, an acoustic Kutta condition is applied at the edge of the area expansion, by imposing the condition that the fluid displacement as well as the derivative of the displacement with respect to $x$ equals zero at $x=0,\ y=h_1$. This gives the following mode matching equation:

$$\underbrace{\begin{pmatrix} -\mathbf{Q}_1^- & \mathbf{Q}_2^+ \\ \mathbf{0} & \mathbf{V}_2^+ \\ -\mathbf{V}_1^- & \mathbf{P}_2^+(1:N_1,:) \\ -\mathbf{P}_1^- & \mathbf{V}_{\mathbf{nf}}^+ \\ \mathbf{0} & \mathbf{V}_{\mathbf{nf}}^+\mathbf{k}_2^+ \end{pmatrix}}_{\mathbf{S_1}} \begin{pmatrix} \mathbf{C}_1^- \\ \mathbf{C}_2^+ \end{pmatrix} = \underbrace{\begin{pmatrix} \mathbf{Q}_1^+ & -\mathbf{Q}_2^- \\ \mathbf{0} & \mathbf{V}_2^- \\ \mathbf{V}_1^+ & -\mathbf{P}_2^-(1:N_1,:) \\ \mathbf{P}_1^+ & -\mathbf{V}_{\mathbf{nf}}^- \\ \mathbf{0} & -\mathbf{V}_{\mathbf{nf}}^-\mathbf{k}_2^- \end{pmatrix}}_{\mathbf{S_2}} \begin{pmatrix} \mathbf{C}_1^+ \\ \mathbf{C}_2^- \end{pmatrix}. \tag{9}$$

Here, the columns of matrices $\mathbf{Q}$, $\mathbf{V}$, $\mathbf{P}$, and $\mathbf{V_{nf}}$ contain the eigenmodes $\mathbf{Q}_e$, $\mathbf{V}_e$, $\mathbf{P}_e$, and that of $V_{\mathrm{noflow}}$, respectively. Vectors $\mathbf{C}$ contain the coefficients of the modes. Additional subscripts 1 and 2 refer to the duct region. A discrimination in the direction of propagation of the modes is made by superscripts $+$ and $-$. Matrices $\mathbf{k_2}$ contain the wavenumbers in duct 2 on their diagonal. The scattering matrix can be obtained by $\mathbf{S} = \mathbf{S_1}^{-1}\mathbf{S_2}$. The reflection and transmission coefficients of the plane waves are given by

$$R^+ = \mathbf{S}(1,1), \quad T^- = \mathbf{S}(1,2N_1+1),$$
$$T^+ = \mathbf{S}(N_1+1,1), \quad R^- = \mathbf{S}(N_1+1,2N_1+1). \tag{10}$$

### 2.1. Discerning the modes

When the modes and their wavenumbers are calculated, the direction of propagation is in fact not known. This especially becomes a relevant issue when an unstable hydrodynamic mode may be present, since it can be confused with an evanescent acoustic mode decaying in the $-x$ direction, as both (can) have a wavenumber with positive real and imaginary part. Formally, in order to determine the direction of propagation of modes, two causality criteria are available, viz. the Briggs–Bers formalism [14,15] and the Crighton–Leppington formalism [16,17]. In both cases the wavenumbers of the modes are traced while letting the angular frequency $\omega$ go from a complex value to its eventual real value. In the Briggs–Bers formalism $\mathrm{Re}(\omega)$ is kept constant while $\mathrm{Im}(\omega)$ runs from $-\infty$ to 0. In the Crighton–Leppington formalism $|\omega|$ is fixed and $\arg(\omega)$ runs from $-\frac{1}{2}\pi$ to 0. For the current $\exp(\mathrm{i}(\omega t - kx))$ convention, if a wavenumber originates in the lower complex plane, the mode is right running, if it originates in the upper complex plane the mode propagates to the left. This implies that if the wavenumber crosses the real axis the mode is unstable. In this way evanescent acoustic modes and unstable (exponentially growing) hydrodynamic modes can be distinguished. Note here that for real frequencies the wavenumbers are found in complex conjugate pairs. Furthermore, neutral hydrodynamic modes and propagating acoustic modes, which both have purely real wavenumber, can be discerned by the fact that the propagating acoustic modes have $k/k_0 \leq 1$, whereas for the neutral hydrodynamic modes $k/k_0 \geq 1/M_{\max}$, with $M_{\max}$ the maximum Mach number of the mean flow.

### 2.2. Steady and acoustic Kutta conditions

The mode matching at an area expansion in a duct has been discussed for three mean flow configurations: for non-uniform flow, where mean flow velocity is zero at the edge of the area discontinuity, and for uniform mean flow in Ref. [1], and in the above for non-uniform flow with a slip velocity at the edge. In the present method viscosity of the fluid is neglected, however, the physical effect of viscosity near the edge of the area expansion can be included by applying steady and/or unsteady (acoustic) Kutta conditions. In the preceding, the steady Kutta condition was imposed for the mean flow in all three configurations, by assuming that the mean flow profile in the duct upstream of the area expansion continues unaltered downstream of the expansion. This represents free jet formation by flow separation. For the acoustic field the unsteady Kutta condition can, however, only be imposed explicitly for non-uniform mean flow with a slip velocity at the edge and for uniform mean flow.

This means that for the non-uniform flow configuration the effect of viscosity is included in the way it affects the boundary layer profile of the mean flow. Here, the mean flow also satisfies the no slip condition at the wall due to viscosity.

Clearly other effects of viscosity, such as turbulent mixing downstream of the expansion, are neglected. For the acoustic field, however, the effect of viscosity cannot be explicitly accounted for. For the uniform mean flow configuration the effect of viscosity is included for the mean flow and the acoustic field only near the edge, where both Kutta conditions are applied. For the configuration of non-uniform mean flow with slip velocity at the wall the effect of viscosity is taken into account because it determines the mean flow profile. Next to this the slip velocity enables us to include the effect of viscosity for the acoustic field near the edge by applying an acoustic Kutta condition.

When modelling the acoustic behaviour of, in this case, an area expansion in a duct, or any geometry containing an edge, the validity of an acoustic Kutta condition in fact depends on the exact physical configuration, which is modelled. The Kutta condition namely cancels the unphysical singularity in the (acoustic) flow field at the edge. However, this singular behaviour is an outcome of the fact that in the model the edge is sharp. In reality the edge will not be infinitely sharp, but is rounded with a certain radius of curvature $r_e$. The question whether or not to apply the acoustic Kutta condition in the model depends on the ratio of certain variables in the physical situation. In the absence of mean flow, the acoustic Kutta condition is related to vortex shedding which occurs if the acoustic boundary layer thickness, given by

$$\delta_{\mathrm{ac}} = \sqrt{\frac{2\nu}{\omega}}, \tag{11}$$

with $\nu$ the kinematic viscosity, and the amplitude of the acoustic fluid displacement, $|u'|/\omega$, are both larger than the edge's radius of curvature $r_e$, see e.g. Disselhorst [18]. In fact the detailed prediction of flow separation is extremely complex. It involves the competition between adverse pressure gradient along the wall and the diffusion of momentum from the main flow towards the fluid in the boundary layer [19]. In the case of a laminar flow separation such as when there is no main flow, the prediction of flow separation is already very complex. When the main flow is turbulent there is no simple analytical model available to predict flow separation from a smoothly curved wall. Nevertheless, also when there is a mean flow, it can be expected that there is no acoustically induced flow separation if the acoustic boundary layer thickness and the particle displacement are both small compared to the radius of curvature $r_e$ of the edge. This, however, depends on the coupling between the acoustic flow and the steady flow, which is determined by the ratio of acoustic boundary layer thickness $\delta_{\mathrm{ac}}$ and viscous sublayer $\delta^+$ of the upstream main flow profile:

$$\delta^+ = \frac{\nu}{u_{\mathrm{fric}}}. \tag{12}$$

Here, $u_{\mathrm{fric}}$ is the friction velocity given by

$$u_{\mathrm{fric}} = \sqrt{\frac{\tau_w}{\rho_0}}, \tag{13}$$

with $\tau_w$ the shear stress at the wall, and $\rho_0$ the mass density. The interaction between the acoustic field and the main flow in a pipe has been studied by Ronneberger [20], Peters [21] and Howe [22].

When $\delta_{\mathrm{ac}}/\delta^+ < 10$ it appears that the acoustical visco-thermal damping is accurately described by assuming that the acoustically induced viscous losses are independent of the main flow. One could therefore assume in such a case that, if the edge radius $r_e$ is larger than $\delta_{\mathrm{ac}}$ and the acoustical particle displacement, the acoustic Kutta condition should not be applied. This corresponds to the present model assuming zero main flow velocity at the edge of the duct discontinuity, $U(0) = 0$.

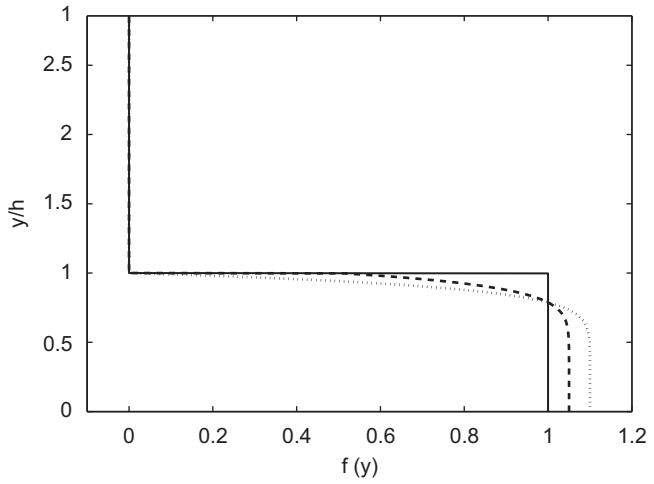


**Fig. 2.** Flow profile $f(y)$ in duct 2 as given by Eq. (14) with flow profile parameter $m = 10$ and with different values of slip coefficient $f_{\mathrm{int}}$. Dotted line: $f_{\mathrm{int}} = 0$, dashed line: $f_{\mathrm{int}} = 0.5$, solid line: $f_{\mathrm{int}} = 1$. For $f_{\mathrm{int}} = 0$ the flow is partly non-uniform without velocity jump, for $f_{\mathrm{int}} = 1$ the flow becomes partly uniform.

When $\delta_{ac}/\delta^+ > 10$ there appears to be a strong coupling between the turbulent main flow and the acoustic field. This coupling is described by Ronneberger [20] by an elegant model in which the shear waves in the acoustical viscous boundary layer reflect at the edge of the turbulent core flow (at $y \simeq 12\delta^+$) which acts as a hard wall, due to the large turbulent eddy viscosity. In the limit of $\delta_{ac}/\delta^+ \gg 10$ the model of Ronneberger [20] simplifies into a quasi-steady coupling between the acoustic field and the main flow, because the shear-wave propagation time in the viscous sublayer can be neglected compared to the acoustical oscillation period. As we apply a steady Kutta condition on the main flow and there is a strong coupling with the acoustic flow, we expect that in such a case an acoustic Kutta condition should be applied in order to describe the modulation of the vorticity shedding by the acoustic field. If we expect the non-uniform main flow profile to have a significant impact and we do not want to restrict ourselves to a frictionless theory for the acoustic field we have to employ the configuration with a slip flow at the duct wall and consequently a velocity discontinuity at the edge of the free jet, downstream of the separation point. The magnitude of this assumed slip flow velocity is the actual main flow velocity at the edge of the viscous sublayer, $U(12\delta^+)$.

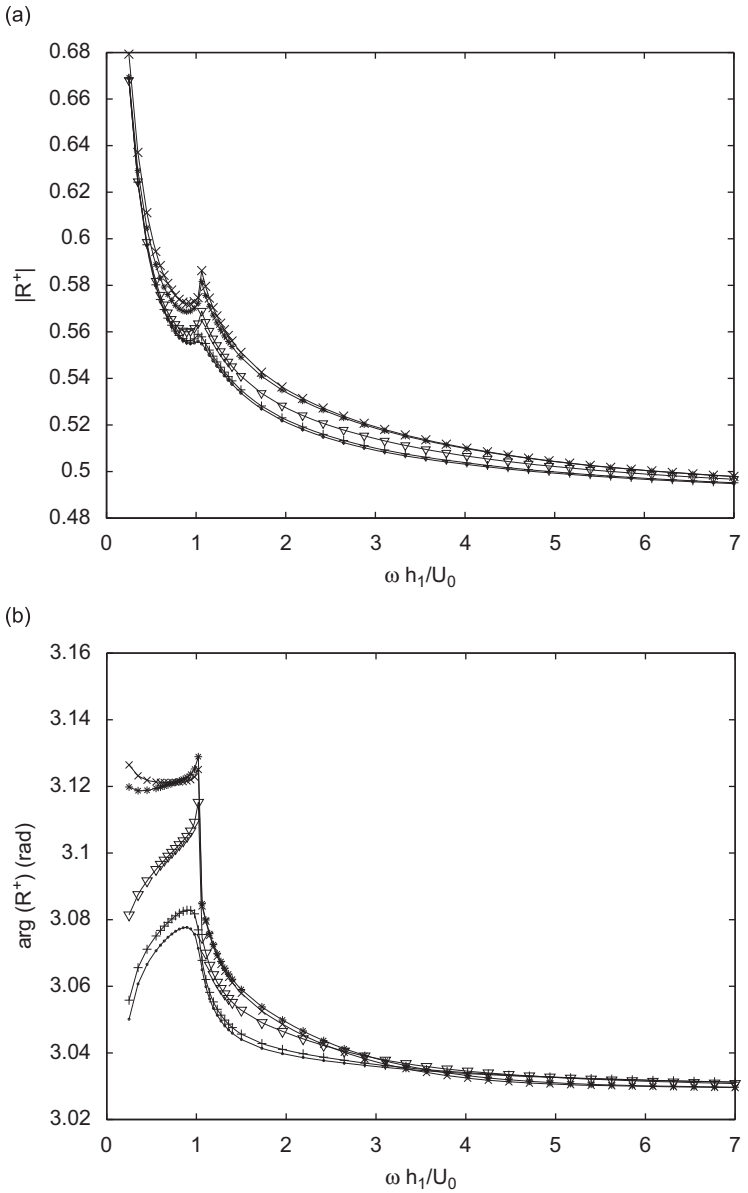


**Fig. 3.** Magnitude (a) and phase (b) of the downstream plane wave pressure reflection coefficient $R^+$ at an area expansion versus Strouhal number $\omega h_1/U_0$ with $\omega h_1/c_0 = 0.11$, $h_1/h_2 = 0.35$, $N_1 = 70$ and $N_2 = 200$. Mean flow profile is given by Eq. (14), where $m = 10$ and $f_{int} = 0$ ($\times$), $f_{int} = 0.1$ ($*$), $f_{int} = 0.5$ ($\nabla$), $f_{int} = 0.9$ ($+$) and $f_{int} = 1$ ($\cdot$), respectively. For $f_{int} = 0$ no Kutta condition is applied in the mode matching procedure, for other values of $f_{int}$ a Kutta condition is applied. Quasi-stationary solution without mean flow is $R^+ = -0.4815$.

In the following, the influence of the mean flow profile configuration—non-uniform, non-uniform with slip, or uniform—and the associated possible application of an acoustic Kutta condition, on the scattering at an area expansion will be investigated. This will provide some insight in the effect of applying an acoustic Kutta condition in the first place, without discussing the issue of which configuration is physically most relevant.

## 3. Influence of flow profile

Consider a non-uniform velocity profile with slip velocity at the upper wall of duct 1, as was shown in Fig. 1. The mean flow continues unaltered into duct 2, resulting in a partly non-uniform flow with velocity jump at the mean flow to no mean flow interface. Here, we take the following profile function:

$$f(y) = \begin{cases} \dfrac{m+1}{m}(1-f_{\mathrm{int}})\left(1-\left(\dfrac{y}{h_1}\right)^m\right)+f_{\mathrm{int}}, & 0 \le y \le h_1, \\ 0, & h_1 < y \le h_2, \end{cases} \tag{14}$$

where $m$ is a profile parameter setting the steepness of the profile. The parameter $f_{\mathrm{int}}$ sets the slip velocity or velocity jump, and will be denoted as the slip coefficient. If $f_{\mathrm{int}} = 0$ the slip velocity is zero, if $f_{\mathrm{int}} = 1$ the mean flow profile is uniform, and

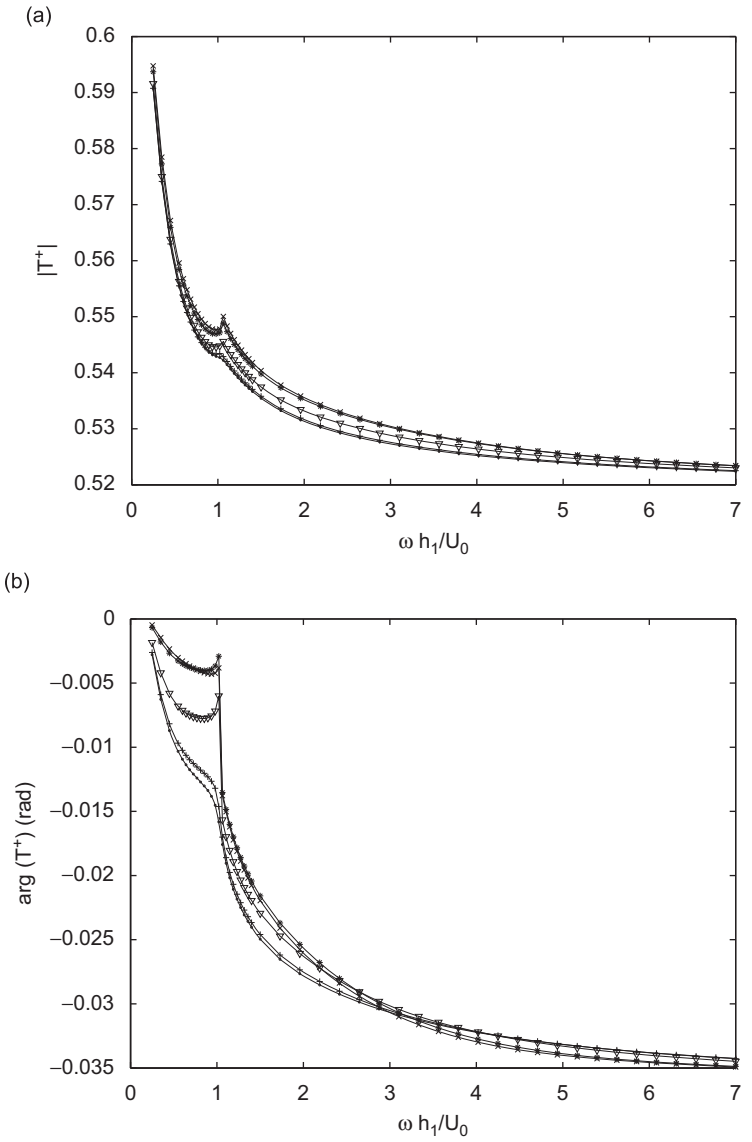


**Fig. 4.** Magnitude (a) and phase (b) of the downstream plane wave pressure transmission coefficient $T^+$ for configurations as in Fig. 3. Quasi-stationary solution without mean flow is $T^+ = 0.5185$.

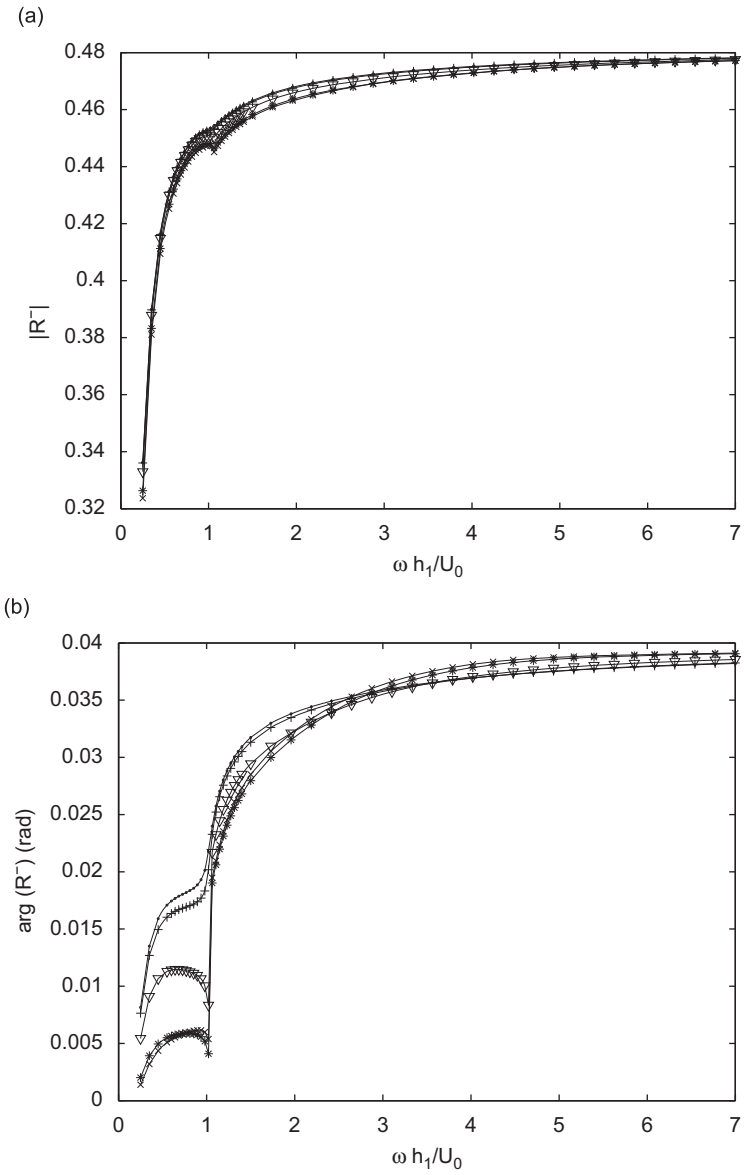


**Fig. 5.** Magnitude (a) and phase (b) of the upstream plane wave pressure reflection coefficient $R^-$ for configurations as in Fig. 3. Quasi-stationary solution without mean flow is $R^- = 0.4815$.

the shear layer in duct 2 becomes infinitely thin. For $f_{\text{int}} = 0$ the profile resembles that of a free jet flow, see Ref. [1]. The average of $f(y)$ in duct 1 equals unity, such that $M_0$ is the mean Mach number according to the definition $M(y) = M_0 f(y)$. Fig. 2 shows the flow profile, Eq. (14), in duct 2 for $m = 10$ and $f_{\text{int}} = 0$, 0.5, and 1. The ratio of duct heights is taken $h_1/h_2 = 0.35$. Calculations for the scattering matrix of an area expansion with $h_1/h_2 = 0.35$ and the above flow profile function with $m = 10$ are performed for different values of the slip coefficient $f_{\text{int}}$, namely $f_{\text{int}} = 0$, 0.1, 0.5, 0.9, and 1. The Helmholtz number on duct height $h_1$ is fixed at $\omega h_1/c_0 = 0.11$, while the mean Mach number $M_0$ is varied. The number of points is $N_1 = 70$ in duct 1 and $N_2 = 200$ in duct 2. For $f_{\text{int}} = 0$, the mean flow is (piece-wise) non-uniform, and the multimodal analysis is performed accordingly as described in Ref. [1] without application of an acoustic Kutta condition. For $f_{\text{int}} = 1$ the mean flow is (piece-wise) uniform, here an acoustic Kutta condition is thus applied in the corresponding multimodal method. For intermediate values, $0 < f_{\text{int}} < 1$, the mean flow in duct 2 is partly non-uniform with a slip velocity at the flow/no flow interface. The multimodal method is performed accordingly for these cases, with thus again explicit application of the acoustic Kutta condition. Results for the plane wave pressure reflection and transmission coefficients as a function of Strouhal number $\omega h_1/U_0$, with $U_0 = M_0 c_0$, are shown in Figs. 3–6.

The effect of going from a uniform flow profile to a non-uniform profile is here to increase the magnitude of the reflection and transmission coefficients except for $R^-$, of which the magnitude is decreased. Especially the magnitudes of

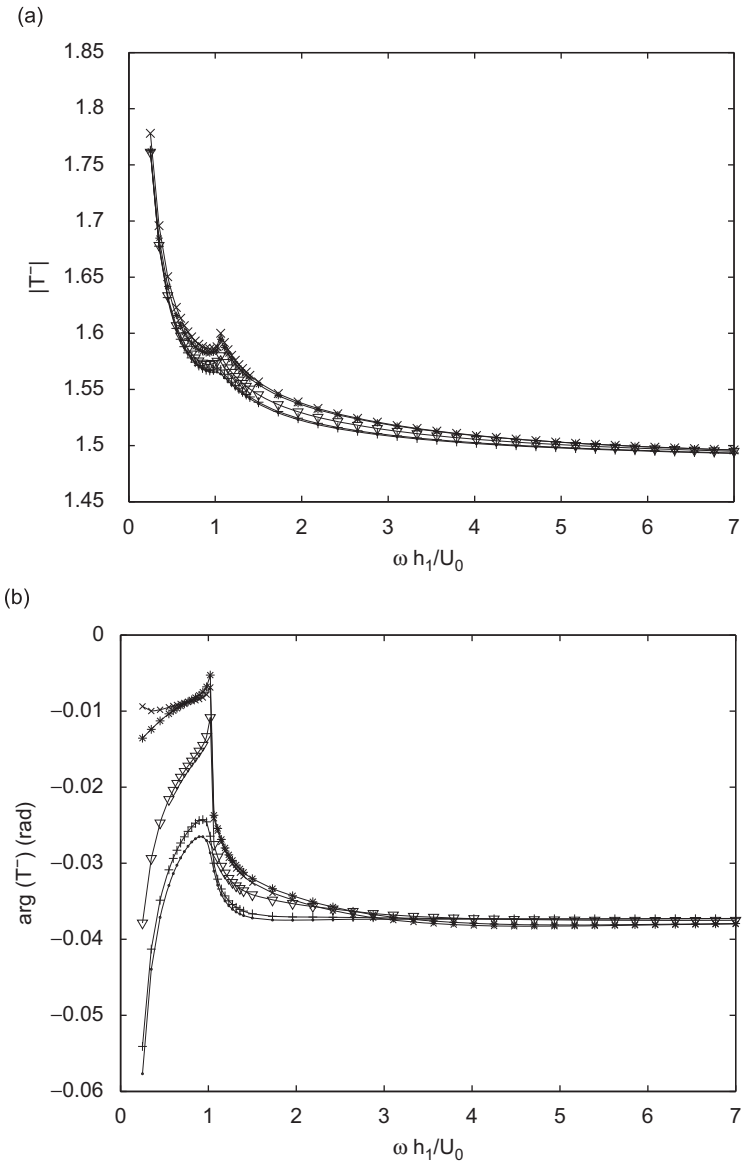


**Fig. 6.** Magnitude (a) and phase (b) of the upstream plane wave pressure transmission coefficient $T^-$ for configurations as in Fig. 3. Quasi-stationary solution without mean flow is $T^- = 1.4815$.

the reflection and transmission coefficients change smoothly as the flow profile is gradually changed. Results for $f_{\text{int}} = 0.1$, giving a non-uniform flow with a small slip velocity in the shear layer, are nearly the same as those for $f_{\text{int}} = 0$, where the slip velocity vanishes. This indicates that application of the Kutta condition in the first case does not have a significant effect on the results compared to the latter case where the Kutta condition is not imposed. Also for $f_{\text{int}} = 0.9$ results are almost the same as for $f_{\text{int}} = 1$. For $f_{\text{int}} = 0.9$ neutral hydrodynamic modes are obtained, whereas in the $f_{\text{int}} = 1$ case, for which mean flow is uniform, they are absent. Therefore, it can be concluded that any effect of the neutral hydrodynamic modes vanishes smoothly as the flow profile is gradually changed from non-uniform to uniform.

Furthermore, the imaginary part of the wavenumber of the unstable hydrodynamic mode in duct 2 (i.e. the growth rate of the hydrodynamic instability) is shown in Fig. 7. For non-uniform flow without velocity jump in the shear layer, $f_{\text{int}} = 0$, the hydrodynamic instability vanishes above a certain Strouhal number. This behaviour is also typically found for free shear layers with finite thickness, see e.g. Michalke [23]. For other values of $f_{\text{int}}$ hydrodynamic instability always occurs due to the velocity jump in the shear layer. Consequently, for Strouhal number larger than about 3 the growth rate of the hydrodynamic instability found for $f_{\text{int}} = 0.1$ begins to differ significantly from that found for $f_{\text{int}} = 0$. Nevertheless, the corresponding results for the reflection and transmission coefficients, Figs. 3–6, are also practically the same for these higher Strouhal numbers. The effect of the hydrodynamic instability, and in particular the non-vanishing of it, is thus

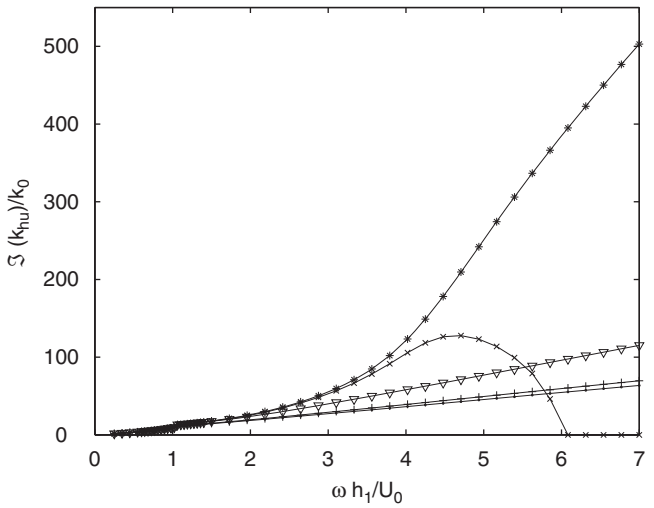


**Fig. 7.** Imaginary part of the wavenumber $k_{hu}$ of the hydrodynamic instability (i.e. growth rate) in duct 2 of the area expansion geometry scaled to $k_0 = \omega/c_0$ versus Strouhal number $\omega h_1/U_0$ for $\omega h_1/c_0 = 0.11$. Mean flow profile is given by Eq. (14), where $m = 10$ and $f_{\text{int}} = 0$ ($\times$), $f_{\text{int}} = 0.1$ ($*$), $f_{\text{int}} = 0.5$ ($\nabla$), $f_{\text{int}} = 0.9$ ($+$) and $f_{\text{int}} = 1$ ($\cdot$), respectively.

negligible for high Strouhal numbers. This conclusion was also drawn by Boij and Nilsson [10] and Howe [24]. Moreover, for low and high Strouhal number especially the magnitudes of the reflection and transmission coefficients converge to the same value for all values of $f_{\text{int}}$, indicating insignificance of the mean flow profile in these limits.

## 4. Influence of geometrical ratios

A striking feature is the hump in reflection and transmission found around Strouhal number equal to 1, cf. Figs. 3–6. Here, for the values of $f_{\text{int}}$ equal to 0.5 or less, the phase plots even suggest a sudden jump. This feature may be connected to the behaviour of the hydrodynamic instability, since in the plot of hydrodynamic instability growth rate, Fig. 7, also a hump is seen for all values of $f_{\text{int}}$ around the same Strouhal number. It turns out that this feature only occurs in case of 'asymmetry' in the flow profile, i.e. when in duct 2 of the expansion geometry the mean flow to no mean flow transition is not halfway the duct. This will be illustrated below for both uniform flow and non-uniform flow in 2D rectangular geometry. Note that the hump was also observed by Boij and Nilsson [9,10] in their model calculations for an infinitely thin shear layer in 2D rectangular geometry for the same Helmholtz number $\omega h_1/c_0 = 0.11$ and ratio of heights $h_1/h_2 = 0.35$. They argued that this feature may be connected to a strong interaction between the hydrodynamic mode and (an) acoustic mode(s).

### 4.1. Uniform flow

Fig. 8 shows the imaginary part of the wavenumber of the unstable hydrodynamic mode as a function of Strouhal number $\omega h_1/U_0$ for different ratios of $h_1$ and $h_2$, obtained by modal analysis calculations in case of uniform mean flow. As above, also here $\omega_* = \omega h_1/c_0 = 0.11$. The number of points in duct 1 is fixed at $N_1 = 70$, the total number of points $N_2$ is thus determined by the ratio $h_1/h_2$. Indeed, the dependence of the (imaginary part of the) hydrodynamic wavenumber on the Strouhal number strongly varies with $h_1/h_2$ ratio. For Strouhal numbers larger than about 2 all results for $h_1/h_2 \leq 0.5$ coincide. The results for $h_1/h_2 = 0.7$ only coincide with those for other $h_1/h_2$ ratios above a Strouhal number of approximately 5.5.

The hydrodynamic instability is also calculated for the case of incompressible flow. From Rayleigh's equation, see e.g. Rayleigh [25] and Drazin and Reid [26], the incompressible solution is found:

$$P_{hu}(y_*) = \begin{cases} A\cosh(k_{hu*}y_*), & 0 \leq y_* \leq 1, \\ B\cosh(k_{hu*}(y_* - h_{2*})), & 1 \leq y_* \leq h_{2*}, \end{cases} \tag{15}$$

with $h_{2*} = h_2/h_1$, and $A$ and $B$ coefficients determined by the wavenumber $k_{hu*}$. The wavenumber is found by demanding continuity of pressure and displacement over the shear layer at $y = h_1$, giving

$$\frac{\tanh(k_{hu*})}{(\omega_* - M_0 k_{hu*})^2} = \frac{\tanh(k_{hu*}(1 - h_{2*}))}{w_*^2}. \tag{16}$$

This equation has to be solved numerically. The results obtained by modal analysis for ratios $h_1/h_2 = 0.35$ and 0.5, cf. Fig. 8, are compared to the incompressible solution, Eq. (16), in Fig. 9. The incompressible solutions for the hydrodynamic

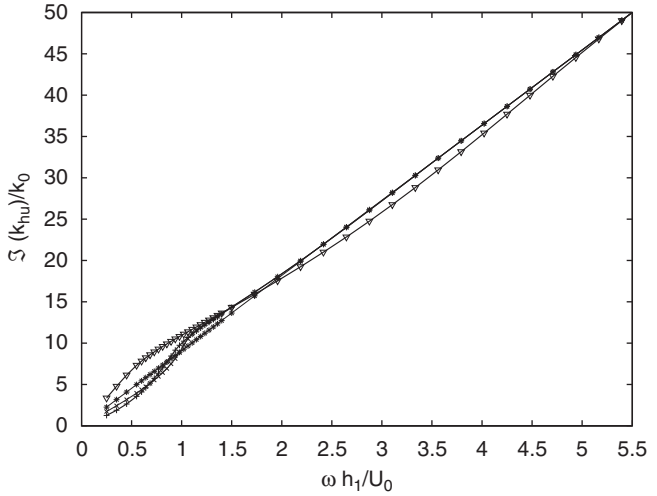


**Fig. 8.** Imaginary part of the wavenumber $k_{hu}$ of the hydrodynamic instability (i.e. growth rate) in duct 2 of the area expansion geometry scaled to $k_0 = \omega/c_0$ for partly uniform mean flow as a function of Strouhal number $\omega h_1/U_0$. Modal analysis calculations with $\omega h_1/c_0 = 0.11$ and $N_1 = 70$. $h_1/h_2$ ratios are $h_1/h_2 = 0.175$ (+), $h_1/h_2 = 0.35$ (×), $h_1/h_2 = 0.5$ (∗), and $h_1/h_2 = 0.7$ (∇).

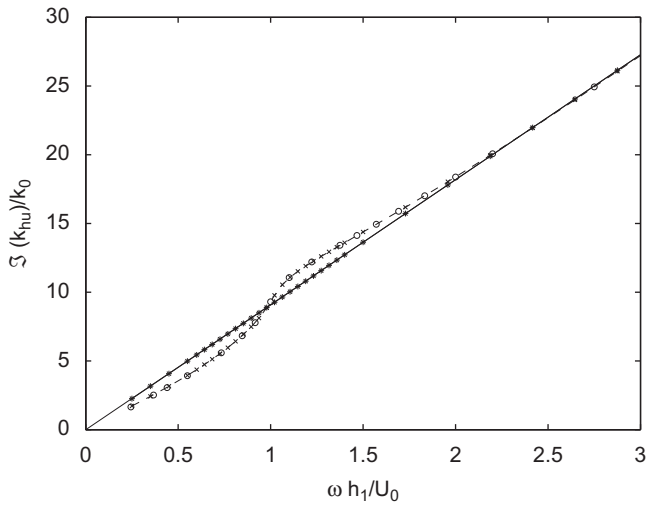


**Fig. 9.** Imaginary part of the wavenumber of the hydrodynamic instability (i.e. growth rate) in duct 2 of the area expansion geometry scaled to $k_0 = \omega/c_0$ for partly uniform mean flow as a function of Strouhal number $\omega h_1/U_0$. Modal analysis calculations with $\omega h_1/c_0 = 0.11$ and $N_1 = 70$. $h_1/h_2$ ratios are $h_1/h_2 = 0.35$ (×) and $h_1/h_2 = 0.5$ (∗). Comparison with the incompressible solution is made: ◦ markers: $h_1/h_2 = 0.35$, solid line: $h_1/h_2 = 0.5$.

wavenumber are close to the results of the compressible modal analysis. This suggests that the observed behaviour of the hydrodynamic instability really is an effect related to the area expansion ratio $h_1/h_2$, regardless the presence of acoustic modes.

The magnitude and phase of the downstream plane wave pressure reflection coefficient $R^+$ at the area expansion with uniform flow are shown in Fig. 10 for the different $h_1/h_2$ ratios. The observed hump (i.e. local maximum) in the magnitude and phase of the reflection coefficient for $h_1/h_2 = 0.175$ and 0.35 seems to coincide with the inflexion point in the plot of hydrodynamic instability growth rate versus Strouhal number, cf. Fig. 8. For the other $h_1/h_2$ ratios the dependence of hydrodynamic instability growth rate as well as reflection coefficient on Strouhal number is more smooth.

A more elaborate picture of the influence of the ratio of duct heights $h_1/h_2$ on the eigenmodes is given in Fig. 11. Here, the wavenumbers of the plane wave acoustic modes, the first six higher order evanescent acoustic modes in both directions and the hydrodynamic modes are shown for different Strouhal numbers for $h_1/h_2 = 0.35$ and 0.5. Besides the influence of the expansion ratio on the hydrodynamic modes, discussed above, also the acoustic modes are strongly affected by the expansion ratio. Moving from $h_1/h_2 = 0.5$ to 0.35 the imaginary part of the wavenumber of the evanescent acoustic modes decreases, which means they are less damped. Also for some evanescent acoustic modes the real part of the wavenumber (related to the phase velocity) becomes significant. A clear maximum in the real part of the wavenumber of the first

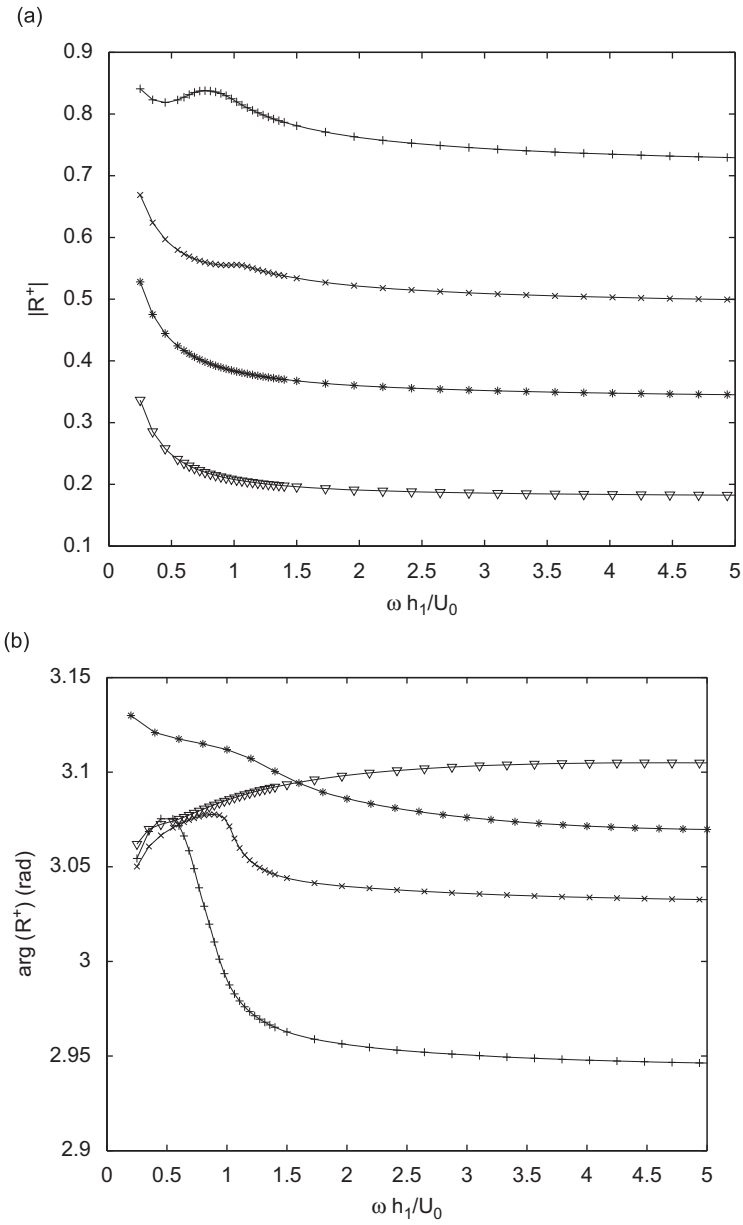


**Fig. 10.** Magnitude (a) and phase (b) of the downstream plane wave pressure reflection coefficient $R^+$ at an area expansion versus Strouhal number $\omega h_1/U_0$ for (partly) uniform flow. Modal analysis calculation with $\omega h_1/c_0 = 0.11$ and $N_1 = 70$. Area expansion ratios are $h_1/h_2 = 0.175$ (+), $h_1/h_2 = 0.35$ ($\times$), $h_1/h_2 = 0.5$ ($*$), and $h_1/h_2 = 0.7$ ($\nabla$).

evanescent acoustic mode is seen around a Strouhal number of 1. Here, the wavenumbers of the first evanescent acoustic mode and the hydrodynamic mode are also closest.

### 4.2. Non-uniform flow

Similarly, the jump seen in the reflection and transmission coefficients for non-uniform flow, cf. Figs. 3–6, is connected to the behaviour of the modes' wavenumbers as a function of the area expansion ratio. For the flow profile, given by Eq. (14), with $f_{\text{int}} = 0$ (no velocity jump in the shear layer) and $m = 10$, the wavenumbers of the modes in downstream duct 2 for several Strouhal numbers $\omega h_1/U_0$ are shown in Fig. 12 for expansion ratios $h_1/h_2 = 0.35$ and 0.5. For Strouhal number close to 1 the wavenumbers of the first higher order evanescent acoustic modes and the hydrodynamic instability modes are very close for the $h_1/h_2 = 0.35$ case compared to the $h_1/h_2 = 0.5$ case. At first sight the traces of the wavenumbers as a

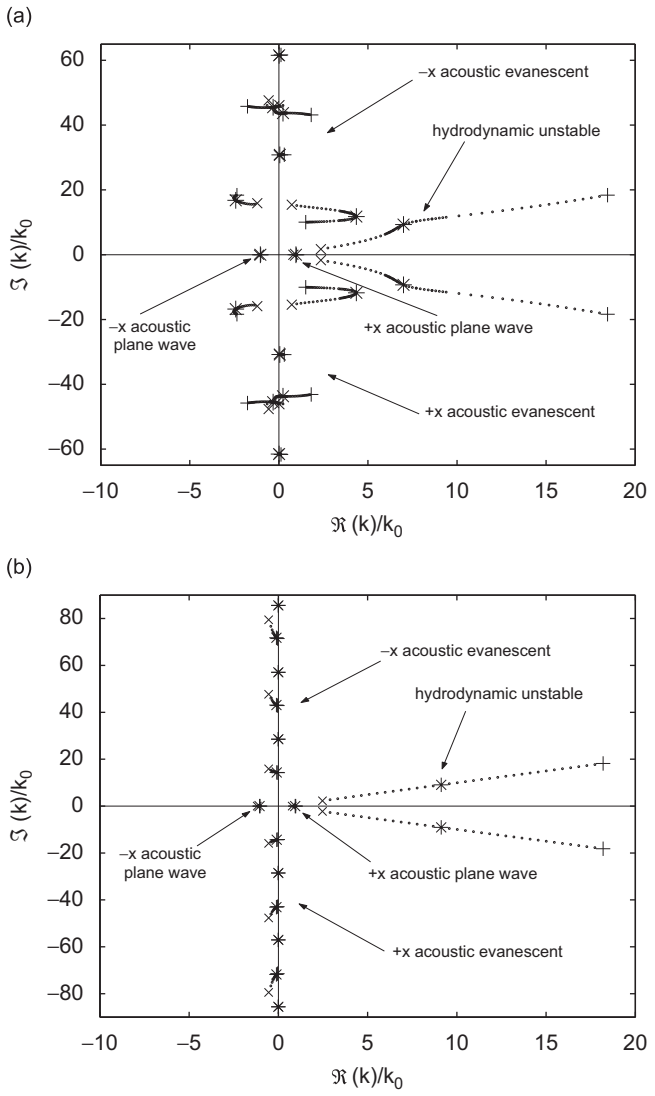


**Fig. 11.** Wavenumbers of the plane wave acoustic modes, the first six higher order evanescent acoustic modes and the hydrodynamic instability modes for different Strouhal numbers $\omega h_1/U_0$ in case of an infinitely thin shear layer. Dimensionless angular frequency and number of points in duct part with flow are fixed at $\omega h_1/c_0 = 0.11$, respectively, $N_1 = 70$. (a) Ratio $h_1/h_2 = 0.35$, (b) ratio $h_1/h_2 = 0.5$. Strouhal numbers are between 0.25 ($\times$ markers) and 2 ($+$ markers), wavenumbers for Strouhal number equal to 1 are indicated by the $*$ markers for all other values by the $\bullet$ markers. Note that for $h_1/h_2 = 0.35$ more points are taken in the vicinity of Strouhal $= 1$.

function of Strouhal number for these modes seem to be well distinguishable for $h_1/h_2 = 0.35$. However, for low Strouhal number the wavenumber of the hydrodynamic instability mode is expected to tend to zero, while for higher Strouhal number at least the real part of the wavenumber is expected to be large compared to the wavenumber of the first higher order evanescent acoustic mode. This would be in contradiction with the two distinguishable traces of the wavenumbers of these modes. Supposedly a jump or exchange occurs between the first higher order evanescent acoustic mode and the hydrodynamic unstable mode at a certain Strouhal number, resulting in the jump in scattering coefficients.

### 4.3. Absolute instability

Since the solution above exhibits a jump it is not analytic, and consequently the causality criteria discussed in Section 2.1 cannot be used. In order to make the solution analytic, and thus causal, a branch-cut in the complex $\omega$- plane would have be to introduced [15]. This branch cut yields an absolute instability. For a similar flow duct model with slip this absolute instability has been studied in more detail by Nilsson and Brander [27]. For uniform flow the solution does not exhibit a jump. However, as discussed by Boij and Nilsson [9,10], and confirmed by the results above, also here interaction between the first higher order acoustic mode and the hydrodynamic mode occurs, giving the observed hump in scattering

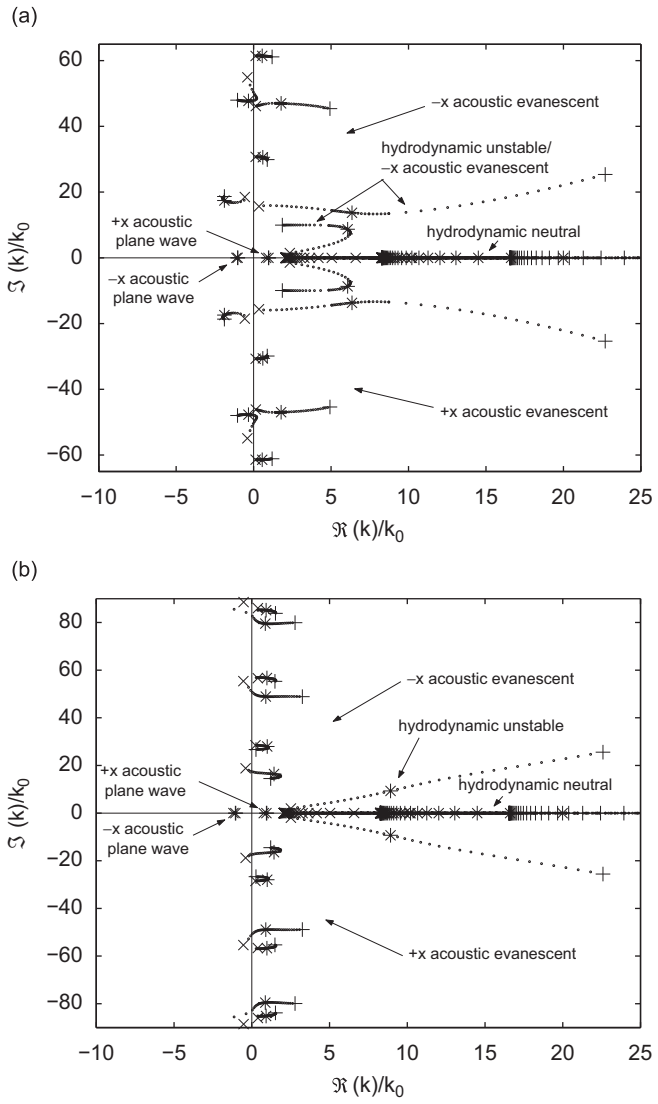


**Fig. 12.** Wavenumbers of the plane wave acoustic modes, the first six higher order evanescent acoustic modes, hydrodynamic instability modes and neutral hydrodynamic modes for different Strouhal numbers $\omega h_1/U_0$ in case of partly non-uniform flow. Flow profile is as given by Eq. (14) with $f_{\text{int}} = 0$ and $m = 10$. Dimensionless angular frequency and number of points in duct part with flow are fixed at $\omega h_1/c_0 = 0.11$, respectively, $N_1 = 70$. (a) Ratio $h_1/h_2 = 0.35$, (b) ratio $h_1/h_2 = 0.5$. Strouhal numbers are between 0.25 ($\times$ markers) and 2 ($+$ markers), wavenumbers for Strouhal number equal to 1 are indicated by the $*$ markers, and for all other values by the $\bullet$ markers. Note that for $h_1/h_2 = 0.35$ more points are taken in the vicinity of Strouhal $= 1$.

coefficients. Nilsson [28] showed that in this case a generalization of the Jones–Morgan theory [17] is needed to establish causality.

Causality analysis according to Section 2.1 indeed shows an apparent jump between the first higher order evanescent acoustic mode and the hydrodynamic unstable mode at a certain Strouhal number. According to the Briggs–Bers formalism [14,15] the jump occurs somewhere between Strouhal number $\omega h_1/U_0 = 1.047$ and 1.048, whereas the Crighton–Leppington [16,17] formalism indicates the jump between Strouhal number $\omega h_1/U_0 = 1.048$ and 1.049, see Figs. 13 and 14 respectively. The traces entering these pictures from the right originate in the lower complex plane, while the traces entering from the left originate in the upper complex plane. This leads to the given classification of the modes. The discrepancy between the two formalisms is an outcome of the different 'mapping' between complex and real frequencies.

The pressure disturbance $P(y)$ of the two modes is shown in Fig. 15 for Strouhal number 1.047. For Strouhal numbers 1.048 and 1.049, where the jump from hydrodynamic unstable to acoustic evanescent and vice versa has occurred (depending on causality criterium formalism), the modes stay virtually the same. Clearly, the two modes are very similar, and a distinction on the basis of their shape could not readily be made.

The apparent jump between acoustic evanescent and hydrodynamic unstable mode coincides with the jump in reflection and transmission coefficients, which occurs at the same Strouhal number, already seen in Figs. 3–6. The result for

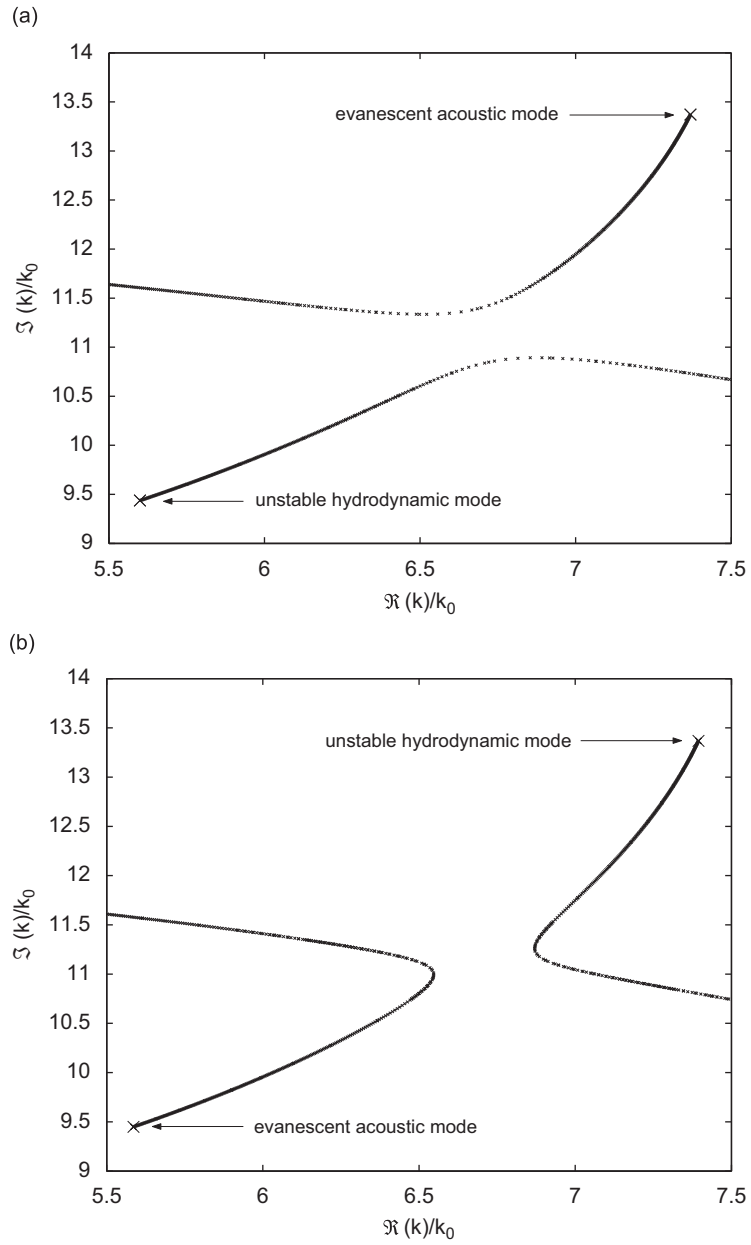


**Fig. 13.** Briggs–Bers causality analysis for the first evanescent acoustic mode and the hydrodynamic instability mode for Strouhal numbers $\omega h_1/U_0 = 1.047$ (a) and $\omega h_1/U_0 = 1.048$ (b) for partly non-unform flow with $h_1/h_2 = 0.35$. Flow profile is as given by Eq. (14) with $f_{\text{int}} = 0$ and $m = 10$. Number of points in duct are $N_1 = 70$ and $N_2 = 200$. Values for final real dimensionless angular frequency $\omega h_1/c_0 = 0.11$ are indicated by the large $\times$ markers. A jump between the two modes occurs.

the downstream reflection coefficient $R^+$ for expansion ratio $h_1/h_2 = 0.35$ is again shown in Fig. 16 together with the result for $h_1/h_2 = 0.5$. The Crighton–Leppington causality analysis is utilized, giving a jump in both magnitude and phase of the reflection coefficient between Strouhal number $\omega h_1/U_0 = 1.048$ and 1.049. For expansion ratio $h_1/h_2 = 0.5$ no apparent jump occurs between the first acoustic evanescent and the hydrodynamic unstable mode, and consequently no jump in reflection coefficient is observed, although a hump can be seen in the phase of the reflection coefficient around Strouhal number 1. This was also seen for an infinitely thin shear layer at the same expansion ratio, cf. Fig. 10.

### *4.4. 2D cylindrical geometry*

The current multimodal method for 2D rectangular geometry can easily be extended to 2D cylindrical geometry, see Ref. [1]. Calculations are carried out for an area expansion in a 2D cylindrical duct carrying uniform mean flow, with

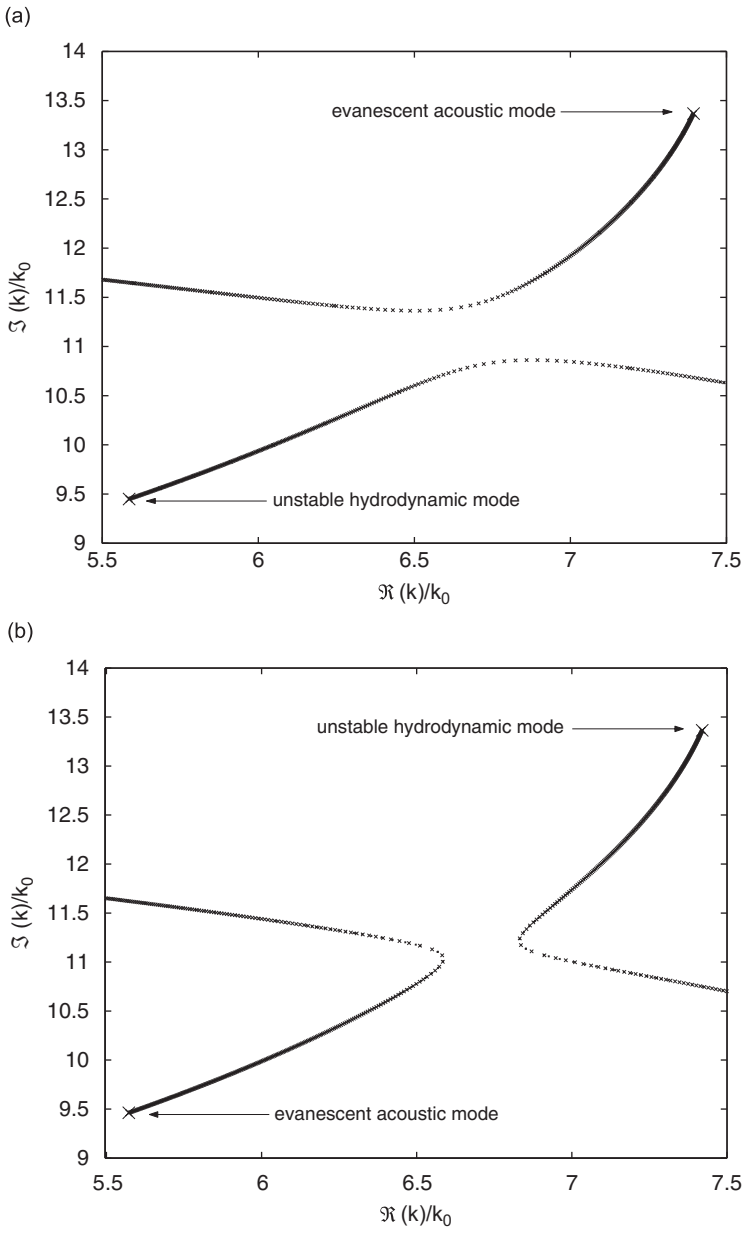


**Fig. 14.** Crighton–Leppington causality analysis for the first evanescent acoustic mode and the hydrodynamic instability mode for Strouhal numbers $\omega h_1/U_0 = 1.048$ (a) and $\omega h_1/U_0 = 1.049$ (b) for partly non-unform flow with $h_1/h_2 = 0.35$. Flow profile is as given by Eq. (14) with $f_{\text{int}} = 0$ and $m = 10$. Number of points in duct are $N_1 = 70$ and $N_2 = 200$. Values for final real dimensionless angular frequency $\omega h_1/c_0 = 0.11$ are indicated by the large $\times$ markers. A jump between the two modes occurs.

Helmholtz number $k_0 r_1 = 0.1$. The reflection and transmission coefficients for the plane acoustic waves for different ratios of duct radii, $r_1$ upstream and $r_2$ downstream of the expansion, are shown in Fig. 17. As for rectangular geometry with ratio of duct heights $h_1/h_2$ less than 0.5, cf. Fig. 10, a hump in the magnitude of downstream reflection coefficient $R^+$ and upstream transmission coefficient $T^-$ is seen around Mach number $M = 0.05$ for ratio of radii $r_1/r_2$ less than 0.5. This feature, which is connected to the behaviour of the modes in the preceding thus depends in the same manner on the ratio of duct heights for rectangular geometry, respectively, duct radii for cylindrical geometry. Consequently, the scaling of the Helmholtz number as proposed by Boij and Nilsson [9] (see also Ref. [1]) in order to compare 2D rectangular and 2D cylindrical geometry with the same area expansion ratio, $h_1/h_2 = r_1^2/r_2^2$, is not valid for all Strouhal numbers, or Mach numbers, in cases where $h_1/h_2 < 0.5$, while $r_1/r_2 > 0.5$.

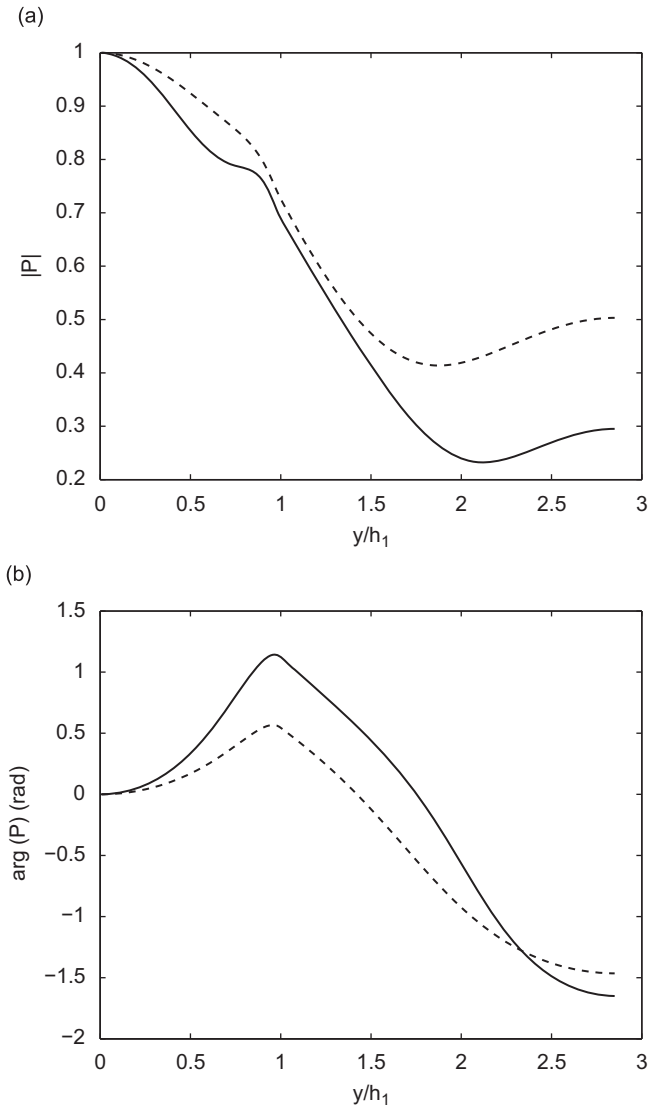


**Fig. 15.** Absolute value (a) and phase (a) for the pressure disturbance $P(y)$ of the two modes with wavenumber $k/k_0 \approx 5.60 + 9.44i$ (dashed line) and $k/k_0 = 7.37 + 13.37i$ (solid line), which jump from hydrodynamic unstable to acoustic evanescent and vice versa. Absolute value and phase at the first discrete point are scaled to unity, respectively, set at zero. Strouhal number is $\omega h_1/U_0 = 1.047$, dimensionless angular frequency $\omega h_1/c_0 = 0.11$. For Strouhal numbers 1.048 and 1.049 the modes are virtually the same. Flow profile is as given by Eq. (14) with $f_{\text{int}} = 0$ and $m = 10$. Number of points in duct are $N_1 = 70$ and $N_2 = 200$.

## 5. Conclusion

Scattering of sound at a sudden area expansion in a duct carrying mean (sheared) flow has been modelled with a multimodal method. Here, the pressure and velocity disturbance field are solved as expansions of eigenmodes both upstream and downstream of the area discontinuity. Mode matching at the area discontinuity, i.e. demanding continuity of the proper acoustic variables, subsequently gives the scattering matrix, which relates all modes. Configurations with uniform mean flow and non-uniform mean flow, for which the method was extensively discussed in our earlier paper [1], can be considered. Next to this a configuration with a non-uniform mean flow profile having a slip velocity at the upstream duct wall, and hence a velocity discontinuity at the edge of the jet in the downstream duct is introduced. As with the uniform mean flow configuration, this configuration allows the application of an acoustic Kutta condition, accounting for the effect of viscosity on the acoustic field near the duct expansion edge. For the normal non-uniform flow configuration, with no slip condition at the wall, no such acoustic Kutta condition can be applied.

It is found that the plane wave scattering coefficients smoothly change when the flow profile is gradually changed from uniform to non-uniform through a non-uniform profile with slip. The non-uniform flow case, where no Kutta condition is applied, is thus the limiting case of non-uniform flow with slip velocity, where a Kutta condition is applied, for slip velocity

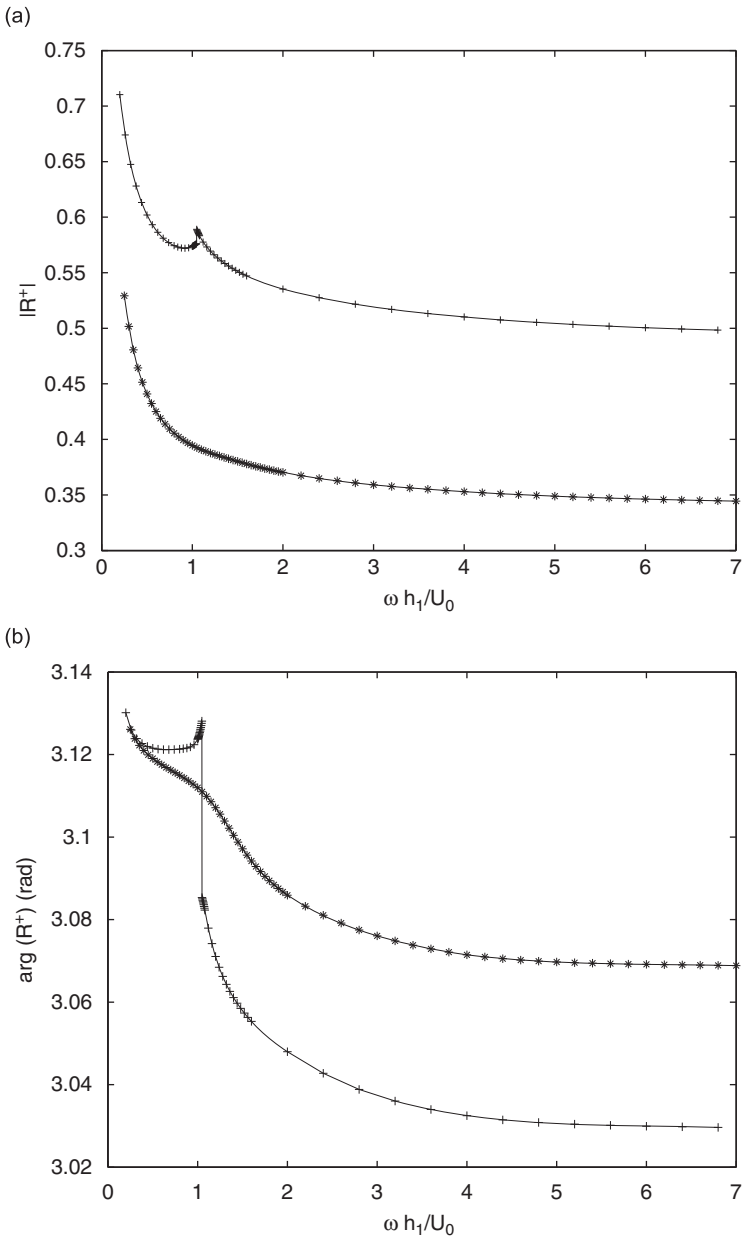


**Fig. 16.** Magnitude (a) and phase (b) of the downstream plane wave pressure reflection coefficient $R^+$ at an area expansion against Strouhal number $\omega h_1/U_0$ for partly non-uniform flow. Flow profile is as given by Eq. (14) with $f_{\text{int}} = 0$ and $m = 10$. Modal analysis calculation with $\omega h_1/c_0 = 0.11$ and $N_1 = 70$. Area expansion ratios are $h_1/h_2 = 0.35$ ($\times$) and $h_1/h_2 = 0.5$ ($*$).

going to zero. The uniform flow case, where neutral hydrodynamic modes vanish, is the maximum slip velocity limit. For high Strouhal numbers no difference is seen in the results for the scattering coefficients obtained for different flow profiles. Also, at low Strouhal numbers the magnitudes of the scattering coefficients are the same for different profiles.

Around a 'critical' Strouhal (or Mach) number, specific behaviour of the scattering coefficients is observed when the ratio of the duct heights $h_1/h_2$ (in 2D rectangular geometry) or radii $r_1/r_2$ (in 2D cylindrical geometry) upstream and downstream of the expansion is less than 0.5. The mentioned effect is found to be connected to an interaction between the first evanescent acoustic mode and the hydrodynamic instability mode.

In case of non-uniform flow, for sufficient low area expansion ratio an apparent exchange or jump between the first evanescent acoustic mode and the hydrodynamic unstable mode occurs at the 'critical' Strouhal number. This in fact implies the occurrence of an absolute instability.

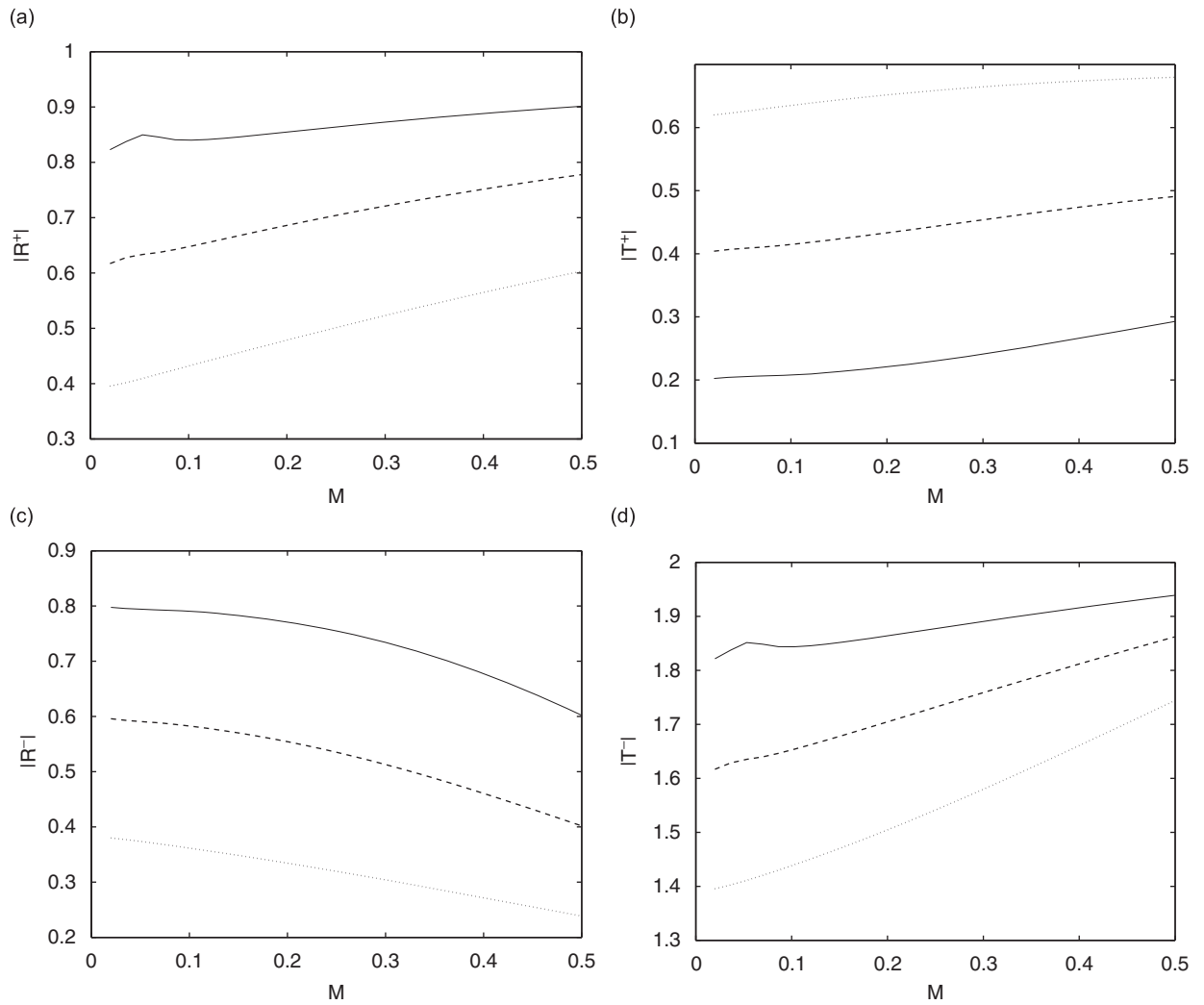


**Fig. 17.** Absolute value of the downstream reflection (a) and transmission (b) coefficients, respectively, upstream reflection (c) and transmission (d) coefficients at an area expansion in a 2D cylindrical geometry for uniform mean flow versus Mach number $M$ for different ratios $r_1/r_2$ of duct radii upstream and downstream of the expansion. Helmholtz number on upstream duct radius is $k_0 r_1 = 0.1$, number of points in upstream duct is $N_1 = 70$. Dotted lines: $r_1/r_2 = 0.67$ ($N_2 = 105$), dashed lines: $r_1/r_2 = 0.5$ ($N_2 = 140$), solid lines: $r_1/r_2 = 0.35$ ($N_2 = 200$).

For the incompressible solution, when only hydrodynamic modes are present, the above-mentioned behaviour is also observed. Due to the (same) dependance of this phenomenon on ratio of duct heights or radii, the Helmholtz number scaling proposed by Boij and Nilsson [9], in order to compare scattering for the same area expansion ratios $h_1/h_2$ in 2D rectangular, and $r_1^2/r_2^2$ in 2D cylindrical geometry, is therefore not accurate for all Strouhal or Mach numbers.

## Acknowledgement

This research was financially supported by the Dutch Technology Foundation STW.

## References

[1] G. Kooijman, P. Testud, Y. Aurégan, A. Hirschberg, Multimodal method for scattering of sound at a sudden area expansion in a duct with subsonic flow, *Journal of Sound and Vibration* 310 (4–5) (2008) 902–922.
[2] Y. Aurégan, M. Leroux, V. Pagneux, Measurement of liner impedance with flow by an inverse method, *10th AIAA/CEAS Aeroacoustics Conference*, AIAA 2004-2838, 2004.
[3] G. Kooijman, Y. Aurégan, A. Hirschberg, Orifice impedance under grazing flow; modal expansion approach, *11th AIAA/CEAS Aeroacoustics Conference*, AIAA 2005-2857, 2005.

[4] G. Kooijman, Acoustical Response of Shear Layers, PhD Thesis, Eindhoven University of Technology, NL, 2007, ISBN-10: 90-386-2182-5, ISBN-13: 978-90-386-2182-1.
[5] P. Testud, Aéro-acoustique des diaphragmes en conduit: sifflement et cavitation (Aeroacoustics of Diafragms in Ducts: Whistling and Cavitation), PhD Thesis, l'Université du Maine, Le Mans, Fr, 2006.
[6] M. Leroux, Propagation acoustique en conduit traité: influence de l'ecoulement sur la propagation avec impédance de paroi (Sound Propagation in Lined Ducts: Influence of Flow on Propagation with Wall Impedance), PhD Thesis, l'Université du Maine, Le Mans, Fr, 2005.
[7] Y. Aurégan, Comportement aero-acoustique basse-frequence d'une expansion (Low Frequency Aeroacoustical Behaviour of an Expansion), 14ème Congrès Français de Mécanique, no. 451, Toulouse, 1999.
[8] Y. Aurégan, A. Debray, R. Starobinski, Low frequency sound propagation in a coaxial cylindrical duct: application to sudden area expansions and to dissipative silencers, *Journal of Sound and Vibration* 243 (3) (2001) 461–473.
[9] S. Boij, B. Nilsson, Reflection of sound at area expansions in a flow duct, *Journal of Sound and Vibration* 260 (3) (2003) 477–498.
[10] S. Boij, B. Nilsson, Scattering and absorption of sound at flow duct expansions, *Journal of Sound and Vibration* 289 (3) (2006) 577–594.
[11] D. Ronneberger, Theoretische und experimentelle Untersuchung der Schallausbreitung durch Querschnittssprünge und Lochplatten in Strömungskanälen (Theoretical and Experimental Investigation of Sound Propagation through Expansions and Diafragms in Flow Ducts), Abschlußbericht Ro 369/11, 12, 14, Drittes Physikalisches Institut der Universität Göttingen, 1987.
[12] S.W. Rienstra, Sound diffraction at a trailing edge, *Journal of Fluid Mechanics* 108 (1981) 443–460.
[13] D.G. Crighton, The Kutta condition in unsteady flow, *Annual Review Fluid Mechanics* 17 (1985) 411–445.
[14] R.J. Briggs, *Electron-Stream Interaction with Plasmas*, MIT Press, Cambridge, 1964.
[15] A. Bers, Space-time evolution of plasma instabilities—absolute and convective. in: A.A. Galeev, R.N. Sudan (Eds.), *Handbook of Plasma Physics: Volume 1 Basic Plasma Physics*, North-Holland Publishing Company, 1983, ISBN 0-444-86645-0.
[16] D.G. Crighton, F.G. Leppington, Radiation properties of the semi-infinite vortex sheet: the initial-value problem, *Journal of Fluid Mechanics* 64 (2) (1974) 393–414.
[17] D.S. Jones, J.D. Morgan, The instability of a vortex sheet on a subsonic stream under acoustic radiation, *Proceedings of the Cambridge Philosophical Society* 72 (1972) 465–488.
[18] J.H.M. Disselhorst, Acoustic Resonance in Open Tubes, PhD Thesis, Universiteit Twente, NL, 1978.
[19] H. Schlichting, *Boundary Layer Theory*, seventh ed., McGraw-Hill, New York, 1979 ISBN 0070553343.
[20] D. Ronneberger, C. Ahrens, Wall shear stress caused by small amplitude perturbations of turbulent boundary-layer flow: an experimental investigation, *Journal of Fluid Mechanics* 83 (3) (1977) 433–464.
[21] M.C.A.M. Peters, A. Hirschberg, A.J. Reijnen, A.P.J. Wijnands, Damping and reflection coefficient measurements for an open pipe at low Mach and low Helmholtz numbers, *Journal of Fluid Mechanics* 256 (1993) 499–534.
[22] M.S. Howe, The damping of sound by wall turbulent shear layers, *Journal of the Acoustical Society of America* 98 (3) (1995) 1723–1730.
[23] A. Michalke, The influence of the vorticity distribution on the inviscid instability of a free shear layer, *Fluid Dynamics Transactions* 4 (1969) 751–760.
[24] M.S. Howe, Attenuation of sound in a low Mach number nozzle flow, *Journal of Fluid Mechanics* 91 (1979) 209–229.
[25] Rayleigh, *The Theory of Sound*, second ed. MacMillan, London, 1929.
[26] P. Drazin, W. Reid, *Hydrodynamic Stability*, Cambridge University Press, Cambridge, 1981 ISBN 0-521-22798-4.
[27] B. Nilsson, O. Brander, The propagation of sound in cylindrical ducts with mean flow and bulk reacting lining—I. Modes in an infinite duct, *Journal of the Institute of Mathematics and its Applications* 26 (1980) 269–298.
[28] B. Nilsson, Instability waves and causality, in: *Mathematical Modelling in Physics, Engineering and Cognitive Sciences*, Vol. 5, pp. 431–449, in: A. Khrennikov (Ed.), *Proceedings of the Conference Foundations of Probability and Physics—2*, June 2002, Växjö University Press.